Analysis of Invariant Funnels in the Circular Restricted Three-Body Problem

Jared Blanchard[(1)], Martin Lo[(2)], Sigrid Elschot[(1)]

[(1)]Stanford University
Palo Alto, CA, USA
Email: jared711@stanford.edu

[(2)]NASA Jet Propulsion Laboratory, California Institute of Technology
Pasadena, CA, USA

***Abstract* – Scientists have identified several ocean worlds, mostly orbiting the outer planets, with large subsurface oceans that could be hospitable to some form of life. Of these worlds, Europa and Enceladus have emerged as the most promising targets. Designing trajectories to such deep space targets requires balancing multiple objectives. Science objectives are limited by fuel and time constraints. Study of the Circular Restricted Three-Body Problem (CR3BP) has allowed mission designers to find very efficient trajectories that arrive in realistic time frames. Dynamical systems theory has been successfully applied to the CR3BP to compute periodic and quasiperiodic orbits, and their invariant manifolds. Here, we review the idea of invariant funnels, which are sets of trajectories that converge in position space to a target point. We describe our method for computing them, which involves selecting initial conditions with parallel velocities, and we review some of their applications to mission design for the ocean worlds. We examine the topology of the CR3BP to identify why the velocity direction is key to the observed funneling behavior.**

I. Introduction

A. Motivation

Water, a fundamental necessity for all known forms of life, serves as the starting point in the quest for extraterrestrial life. Fortunately, within our own solar system, oceans harboring liquid water are not exclusive to Earth. Evidence of subsurface oceans has been observed on several moons orbiting the outer planets, including Europa, Enceladus, Titan, Ganymede, and Callisto [1].

Among these, Europa (a moon of Jupiter) and Enceladus (a moon of Saturn) stand out as the most intriguing targets. Europa is estimated to hold more liquid water than all of Earth's oceans combined, while Enceladus's southern pole features lengthy crevices from which geysers continuously vent water vapor into space. NASA has set a strategic objective to explore these celestial bodies using robotic spacecraft capable of sampling water and detecting signs of life. This ambition is reflected in missions like the upcoming Europa Clipper and the proposed Enceladus Orbilander, as outlined in [2].

Efficient mission design for these distant targets necessitates the application of dynamical systems theory. Originating from Henri Poincaré's investigations into the chaotic dynamics of the three-body problem, dynamical systems theory has been instrumental in astrodynamics and celestial mechanics. When employed in ocean world missions, it facilitates the design of trajectories that optimize fuel consumption and minimize travel time. In dynamical systems theory, periodic and quasiperiodic orbits are the skeleton of the phase space, and their hyperbolic invariant manifolds connect the space together.

B. Circular Restricted Three-Body Problem

The Circular Restricted Three-Body Problem (CR3BP) is a common model used in astrodynamics to model the motion of an infinitesimal particle under the influence of two massive bodies in circular orbits about their mutual barycenter. See [3] for more details on the CR3BP. The equations of motion rely on a single parameter, the mass ratio of the massive bodies $\mu = \mathrm{m}_2/(\mathrm{m}_1 + \mathrm{m}_2)$, where m_1 and m_2 are the masses of the larger and smaller body, respectively. We normalize the units such that the distance between the bodies, their total mass, and their angular velocity are all unity. We use a rotating frame, as shown in Fig. 1, to fix the bodies on the x-axis and make the equations of motion autonomous.

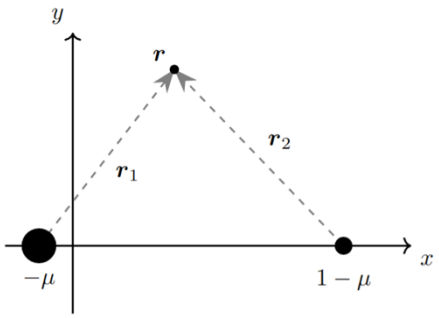

Fig. 1 - CR3BP in the coordinate system of the rotating frame with the larger body at $x = -\mu$ and the smaller body at $x = 1 - \mu$. The origin of the coordinate system is the barycenter of the massive bodies.

The vector $\boldsymbol{r} = [x, y, z]^T$ represents of the position of the spacecraft with respect to the barycenter. The equations of motion in the rotating frame are

$$\ddot{x} = -\left(\frac{1-\mu}{r_1^3}(x+\mu) + \frac{\mu}{r_2^3}(x-1+\mu)\right) + x + 2\dot{y}$$
$$\ddot{y} = -\left(\frac{1-\mu}{r_1^3}y + \frac{\mu}{r_2^3}y\right) + y - 2\dot{x} \quad (1)$$
$$\ddot{z} = -\left(\frac{1-\mu}{r_1^3}z + \frac{\mu}{r_2^3}z\right),$$

where r_1 and r_2 are the distances of the spacecraft from the larger and smaller bodies respectively.

The CR3BP is a Hamiltonian system, with a single integral, the Jacobi constant

$$C = x^2 + y^2 + 2\frac{1-\mu}{r_1} + 2\frac{\mu}{r_2} - (\dot{x}^2 + \dot{y}^2 + \dot{z}^2). \quad (2)$$

For a given C, there exists a zero-velocity surface (ZVS), a locus of points in the position space where the velocity must be zero for the state to have the appropriate Jacobi constant. The ZVS bounds the forbidden region, where motion is not possible.

There are five equilibrium points in the CR3BP, referred to as Lagrange points. There are also diverse families of periodic and quasi-periodic orbits around the Lagrange points. In fact, the phase space is foliated by invariant tori, the hyperbolic manifolds of which provide a structure for designing trajectories between orbits of interest.

The Planar CR3BP (PCR3BP) is a common simplified model that assumes there is no out-of-plane motion (i.e. $z = \dot{z} = 0$. We use it in this work to help build intuition, due to its lower-dimensional state space.

C. *Invariant Funnels*

In previous work [4] [5], we describe invariant funnels, which are sets of trajectories that converge toward some nominal trajectory. We discovered these structures when searching for low-energy trajectories that reach high latitudes on Europa [6] and have since applied them to mission design problems for Europa [7] and Enceladus [8]. We compute invariant funnels by sampling a closed surface of initial conditions around a state on the nominal trajectory, while constraining the velocities (in the xy plane of each sampled state to be parallel to each other. This parallel velocity condition seems to be the key. When these sampled states are integrated backward in time, they spread out in position space, forming a funnel. An example is shown in Fig. 2, in which a ring of points 50 km wide on the surface of Europa is integrated backward.

In terms of nomenclature, we define an invariant funnel as all the trajectories that reach a given region around the final state of a nominal trajectory $\bar{x}(t)$. The final

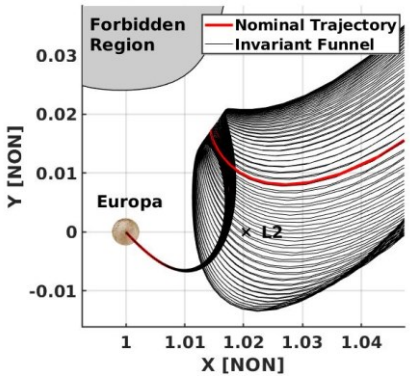

Fig. 2 - An invariant funnel converging in position space around a resonant landing orbit to Europa's north pole.

state is denoted $\boldsymbol{x}^* = (\boldsymbol{r}^*, \dot{\boldsymbol{r}}^*)$. We sample states, $\boldsymbol{x}_i = (\boldsymbol{r}_i, \dot{\boldsymbol{r}}_i)$, along closed curve centered on $\boldsymbol{x}^*$. The xy projection of each $\dot{\boldsymbol{r}}_i$ is parallel and all states share the same Jacobi constant. We refer to these points as the initial boundary of the funnel, denoted $\partial\mathcal{F}_0$, see Fig. 3.

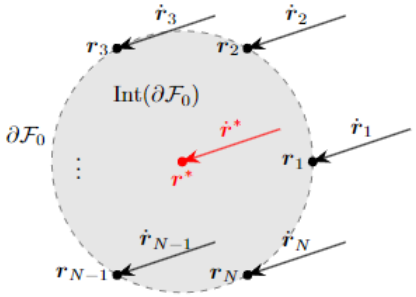

Fig. 3 – Discrete sampling of the initial boundary of an invariant funnel. In this work, we only integrate the boundary

When we integrate the initial boundary backward, it gives us the full boundary of the funnel as a function of time $\partial\mathcal{F}(t)$. For a selected time t, the boundary $\partial\mathcal{F}_t$ remains homeomorphic to the initial boundary, as long as t is not too long and the initial boundary is not too large.

One question that we have had since beginning this work is whether we can define an interior/exterior to the funnels. For example, if we have an arbitrary spacecraft state, can we derive an analytical expression that quickly determines if that spacecraft is inside the funnel? By doing so, we could program a controller to target the interior of the funnel, which is a much larger target than the trajectory itself. The hope is that such an algorithm would be using natural dynamics to improve efficiency.

In our previous work [7], we attempted to approach this problem by integrating a set of trajectories on the funnel boundary with a fixed time step. At each time step, we fit a hyperellipsoid to the corresponding funnel points. Therefore, we had a discrete sampling of time, with a

hyperellipsoid defined at each time step. We defined our spacecraft state in terms of deviations from the time-discretized nominal trajectory, so at each time step, we could plug the deviation from the corresponding nominal trajectory into the equation of a hyperellipsoid to determine if it was "inside" the funnel or not. This was good enough for our simple case study with small funnels and small deviations from a nominal trajectory with pre-defined knot points. We showed that an MPC control scheme can reduce the amount of fuel required by including the approximate funnels as terminal sets. However, we would like to explore the idea of an interior to the funnel more deeply, potentially developing a method to classify whether an arbitrary state, far away from the nominal trajectory, is inside/outside a funnel.

II. Methods

A. *Topology of manifolds*

To divide an N-dimensional space, an $(N-1)$-dimensional surface is required, which can be created by extruding an $(N-2)$-dimensional closed surface through time. Fig. 4 shows an example of a 3D space being divided by a 2D cylinder created by extruding a 1D curve. Note that, to form a surface with an interior and exterior, the direction of extrusion must be transverse to the closed surface on which the initial conditions lie. For example, if the circle in Fig. 4 was extruded straight up and down, there would be no interior. We discuss this idea more in section III.A.

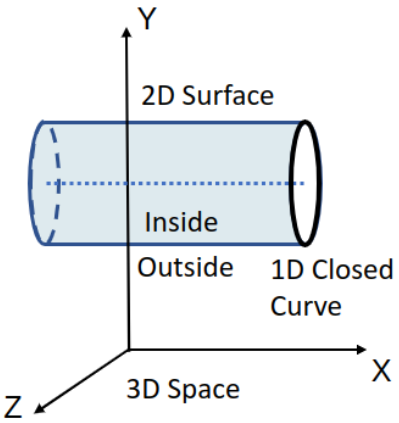

Fig. 5 - An example of a 3D space divided by the 2D extrusion of a 1D closed curve.

In the spatial CR3BP, the phase space is six-dimensional, meaning there is a five-dimensional energy surface (i.e., $N = 5$). with a four-dimensional parallel velocity surface embedded in it, if only the direction of the velocity projected into the xy plane is fixed. Note that, if both angles that define the velocity direction are fixed entirely then the parallel velocity surface is three-dimensional. This doesn't leave us enough dimensions to sample a closed surface of dimension $N-2=3$. However, since it is very difficult to visualize such high dimensional state spaces, we will first work with the PCR3BP to gain more intuition into the problem at hand.

The PCR3BP has two degrees of freedom, meaning the phase space is four-dimensional. By fixing the Jacobi constant, we are left with a 3D energy surface (i.e., $N = 3$). We sample the initial conditions of an invariant funnel such that they all have parallel velocities. This parallel velocity condition defines a 2D surface embedded in the 3D energy surface. On this 2D parallel velocity surface, we sample a 1D ring of points. This gives us a 1D curve that we can extrude to generate a 2D surface that will divide the 3D energy surface. Note that extrusion corresponds to propagation through time here.

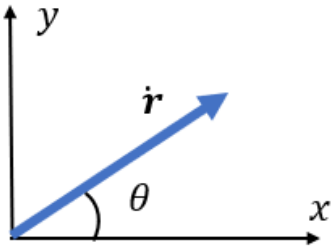

Fig. 4 – All sampled states on an invariant funnel share the same angle θ. In the spatial problem, we allow for variation in the $\dot{z}$ direction.

B. *Cylindrical Isomorphic Mapping*

In his thesis [9], Travis Swenson extended the work of Charles Conley on the topology of transit orbits in the CR3BP. He used a cylindrical isomorphic mapping to better visualize the phase space of the PCR3BP. For a fixed Jacobi constant, only three parameters are needed to uniquely identify a state. However, if using three of the four $(x, y, \dot{x}, \dot{y})$ coordinates, there is ambiguity in the sign of the velocity components. This seemingly innocuous problem becomes more malicious when we realize that trajectories may appear to intersect when plotted in such a phase space. This is remedied by fixing the velocity magnitude $\dot{r} = \sqrt{(\dot{x}^2 + \dot{y}^2)}$ and using the velocity direction in the xy plane, θ, as a coordinate. Topologically speaking, the energy surface is homeomorphic to a ring cross a strip, and this new coordinate system reflects that. The new coordinates are

$$\begin{aligned} x &= x \\ r &= \frac{\tilde{y} - y}{2\tilde{y}} \\ \theta &= atan2(\dot{y}, \dot{x}), \end{aligned} \tag{3}$$

where $\tilde{y}$ is the maximum possible value of y for a given value of x, normally coinciding with the ZVS. Note that the x-coordinate is unchanged and r is simply a scaled version of y. Do not confuse this r with the distance from the barycenter. See Fig. 6 for an illustration of the space. Note that a parallel velocity surface is simply a half-plane with the x-axis as a border.

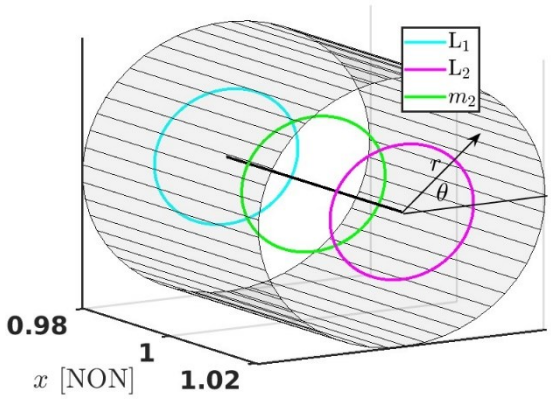

Fig. 6 - Cylindrical space homeomorphic to the energy surface in the PCR3BP. The outer surface corresponds to the lower ZVS while the central line corresponds to the upper ZVS. The Lagrange points and the secondary mass become circles rather than points.

To compute $\tilde{y}$, given values for x and C, we solve for y in (2) assuming the velocity terms are all zero. In other words, we solve for the zeros of

$$f(\tilde{y}; x, C) = x^2 + \tilde{y}^2 + 2\frac{1-\mu}{r_1} + 2\frac{\mu}{r_2} - C. \qquad (4)$$

We use Newton iteration to solve for $\tilde{y}$, starting with $\tilde{y} = 0.02$ as an initial guess in the Jupiter-Europa system with $C = 3.0027$. In Fig. 7, we can see that this initialization converges to the ZVS for x values close to the secondary body, and to a nearly constant value near 0.02 farther away.

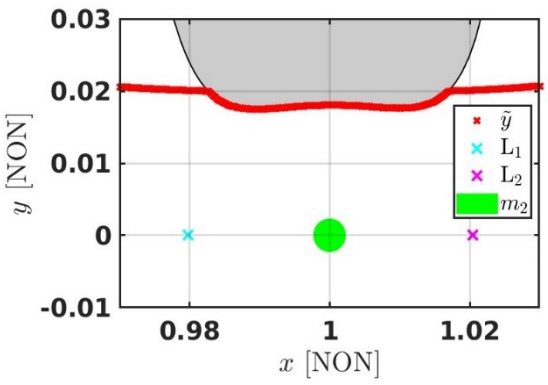

Fig. 7 – The $\tilde{y}$ points shown in red coincide with the ZVS that bounds the forbidden region for x values close to the secondary body. As the ZVS turns sharply away, $\tilde{y}$ slowly increases.

III. Results

A. Funnel in the PCR3BP

We computed an invariant funnel around a resonant landing trajectory in the Jupiter-Europa system, as shown in Fig. 8. The boundary of the funnel, $\partial\mathcal{F}$, is

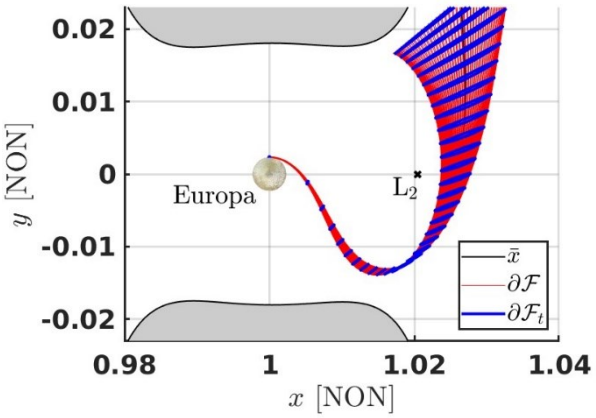

Fig. 8 – Invariant funnel, $\partial\mathcal{F}$(red), around a nominal trajectory, $\bar{x}$ (black),. The nominal trajectory is tangent to the surface of Europa and the velocity is purely in the (negative) x-direction. The evolution of the initial ring (blue) is shown every hour. The total integration time is -64 hours and $C = 3.0027$.

made up by backward propagating a closed curve sampled around the landing site. In this case, the closed curve is a circle of radius 50 km in position space. As we follow the evolution of the circle of initial conditions backward in time, we see that it overlaps itself in the xy projection, as shown in Fig. 9. We know from the uniqueness and existence theorem that trajectories do not cross in the phase space, which becomes immediately clear when we perform the cylindrical isomorphic mapping and plot in the cylindrical space.

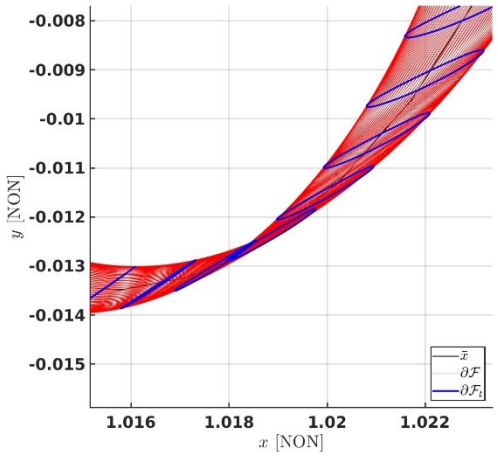

Fig. 9 – A zoomed in view of Fig. 8 showing the ring turning inside out.

B. Funnel in Cylindrical Space

Recall that, in the PCR3BP, the phase space is 4D. Fixing the Jacobi constant yields a 3D energy surface. This surface can be faithfully represented in the (x, r, θ) coordinates as a coaxial pipe. Fig. 10 shows the funnel plotted in this cylindrical space. The initial ring of

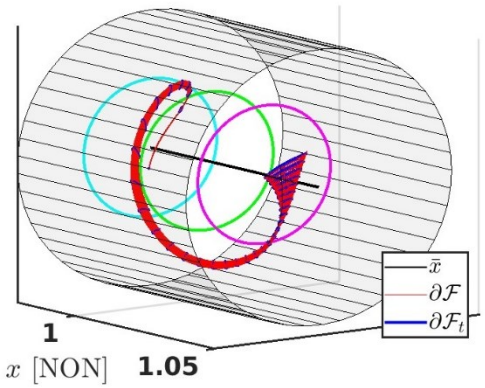

Fig. 10 – The same funnel from Fig. 8 shown in the cylindrical space. We can see that the funnel has width and does not intersect itself.

conditions is sampled on the half-plane representing $\theta = \pi$ and near the green ring representing the secondary body. We note that the initial direction of integration is transverse to the $\theta = \pi$ halfplane, as shown in Fig. 11.

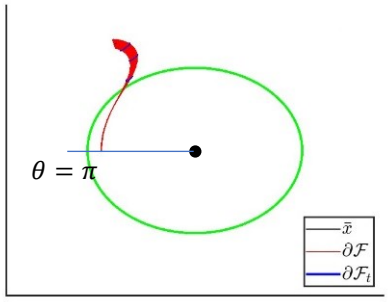

Fig. 11 – A zoomed in view of Fig. 10 shows the transversality of the initial integration direction to the half plane $\theta = \pi$.

C. Transversality Condition

Now that we have the appropriate coordinate system, it is simple to define a transversality condition. As mentioned before, the direction of extrusion (integration) must be transverse to the surface on which the initial conditions lie. In essence, we must make sure that none of the sampled points lie on the same trajectory, in which case we would be extruding an open curve and wouldn't be able to identify an interior. Note that, if the transversality condition holds for our initial boundary, the funnel will not overlap itself. Even as the funnel passes through regions where $\dot{\theta} = 0$, the evolution of the initial boundary will longer share a plane defined by a single θ. In fact, they won't likely lie on a single plane at all.

In our new coordinates, since we sample on a half-plane defined by a fixed θ, the transversality condition can be expressed simply as $\dot{\theta} \neq 0$. Since θ is a function of both $\dot{x}$ and $\dot{y}$, we use the total derivative,

$$\theta = atan2(\dot{y}, \dot{x})$$
$$\frac{d\theta}{dt} = \frac{\partial\theta}{\partial\dot{x}}\frac{d\dot{x}}{dt} + \frac{\partial\theta}{\partial\dot{y}}\frac{d\dot{y}}{dt} \tag{5}$$
$$\dot{\theta} = \frac{\dot{x}\ddot{y} - \dot{y}\ddot{x}}{\dot{x}^2 + \dot{y}^2}.$$

The $\ddot{x}$, and $\ddot{y}$ terms are readily available from the equations of motion. Therefore, when sampling initial conditions for an invariant funnel, a simple check of $\dot{\theta}$ for the nominal landing state to make sure it is not close to zero should suffice. If a large funnel is desired, one should check the entire sample to make sure that they all have the same sign.

We sampled a million points on the energy surface (pipe space) and computed $\dot{\theta}$ at each point. The result is shown in Fig. 12, where we have colored positive and negative values of $\dot{\theta}$ blue and red, respectively. Taking slices of

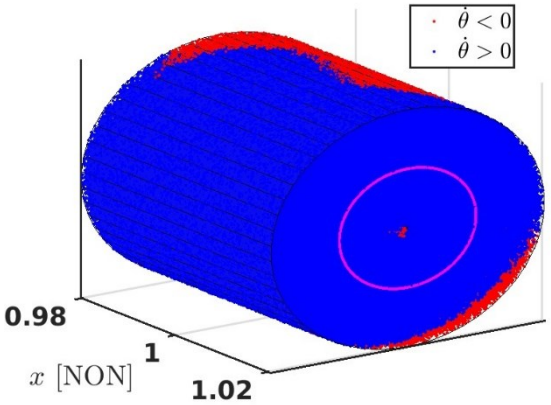

Fig. 12 – The positive and negative values of $\dot{\theta}$ shown in blue and red respectively. The boundary between the red and blue regions is the locus of zeros of (5).

this section at certain values of x gives some insight into the internal structure, as shown in Fig. 13. We can see that the locus of zeros at $x = x_{L_2}$ is small and concentrated near both ZVS (center and outside of the circle). As we move down the x-axis towards the secondary body, we see an arm of negative values stretch out toward the center, completing a circuit around the secondary body itself. As we pass the secondary body, we are left with a mirror situation: an arm of negative values shrinking away from the center now. When we reach $x = x_{L_1}$, we have a small locus of zeros concentrated near the ZVS again.

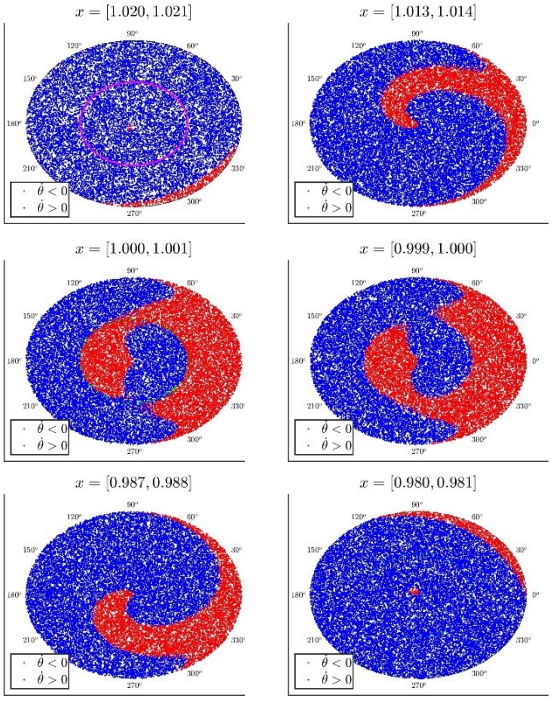

Fig. 13 - Several slices of the object shown in Fig. 12. From left to right, top to bottom, the slices start at L_2 and move towards L_1. The magenta, green, and cyan circles (L_2, m_2, and L_1 respectively) are visible in the top-left, middle-left and bottom-right images. We can see in the middle two images that a large portion of the locus of zeros lies around the secondary body.

D. Topology in the Spatial CR3BP

In the 6D phase space of the spatial CR3BP, the energy surface will have two added dimensions. Fixing the Jacobi constant and allowing freedom in all three of the position coordinates means that the velocity magnitude can be determined uniquely, and two degrees of freedom remain: the azimuth and elevation of the velocity vector. Therefore, the energy surface is homeomorphic to a volume cross a sphere. Obviously, this is a much more complicated space to visualize. Fixing the azimuth, θ of the velocity vector, no longer defines a half-plane, but rather a 4D volume. However, the $\dot{\theta} \neq 0$ condition should still guarantee transversality of the integration direction with that 4D volume. We can sample a hyperellipsoid in that 4D volume as the initial boundary, and if our transversality condition holds, then we will have a 4D surface that divides the 5D energy surface.

Determining whether an arbitrary state lies within that energy surface can be achieved by integrating the state forward and taking a Poincaré section of the passes through the parallel velocity condition. Like in the PCR3BP, there will be multiple passes through the parallel velocity surface, but we can select the passes within some threshold distance to the x-value of the secondary body. Then the point on the Poincaré section can be plugged into the expression defining the closed curve (the equation of a circle or an ellipsoid), which has a well-defined interior.

IV. Conclusion

In conclusion, we have examined the behavior of invariant funnels in the PCR3BP by using a cylindrical isomorphic mapping to visualize the phase space for a fixed Jacobi constant. We have seen that this change of coordinates makes it easy to define a surface of parallel velocity embedded in the energy surface. Furthermore, it enables us to identify a transversality condition that will guarantee that the funnel divides the energy surface into an interior and exterior. We have performed a numerical experiment to identify the regions where the transversality condition may not hold, which seem to pass through the center of the secondary body and approach the ZVS.

Future work will include using jet transport to compute high order approximations of the Poincaré map using just the nominal trajectory. This would allow for an arbitrary state close to the nominal trajectory to be classified as interior/exterior by evaluating a polynomial.

V. References

[1] J. I. Lunine, "Ocean worlds exploration," *Acta Astronautica,* vol. 131, pp. 123-130, 2017.

[2] National Academies of Sciences Engineering and Medicine, "Origins, worlds, and life: a decadal strategy for planetary science and astrobiology 2023-2032," 2022.

[3] V. Szebehely, Theory of orbits, the restricted problem of three bodies, New York, New York: Academic Press Inc., 1967.

[4] J. T. Blanchard, M. W. Lo, D. Landau, B. D. Anderson and S. Close, "Invariant Funnels for Resonant Landing Orbits," in *AAS/AIAA Space Flight Mechanics Conference*, 2021.

[5] J. T. Blanchard, M. W. Lo, D. Landau, B. D. Anderson and S. Close, "New tools for tour design: swiss cheese plot, invariant funnel, and resonant encounter map," in *AAS/AIAA Astrodynamics Specialist Conference*, 2021.

[6] J. T. Blanchard, M. W. Lo, B. D. Anderson and S. Close, "Low Energy Capture into High Inclination Orbits for Ocean Worlds Missions," in *AAS/AIAA Astrodynamics Specialist Conference*, 2020.

[7] J. T. Blanchard and S. Elschot, "Model Predictive Control in the Three-Body Problem Using Invariant Funnels as Terminal Sets," in *AAS/AIAA Astrodynamics Specialist Conference*, Charlotte, NC, 2022.

[8] J. T. Blanchard, M. W. Lo, R. L. Restrepo, D. Landau, B. D. Anderson and S. Elschot, "Using

NRHO Invariant Funnels to Target Enceladus South Pole," in *AAS/AIAA Spaceflight Mechanics Conference*, Austin, TX, 2023.

[9] T. Swenson, "The Topology of Transit Orbits in Multibody Systems with Applications to Dynamical Astronomy and Mission Design," 2018.

[10] D. Pérez-Palau, "Dynamical transport mechanisms in celestial mechanics and astrodynamics problems," 2015.